Electronic Supplementary Material (ESI) for Nanoscale Horizons.
This journal is © The Royal Society of Chemistry 2020

Electronic Supplementary Information

Metal assisted chemical etching of silicon in gas phase: a nanofabrication platform for X-ray optics

Lucia Romano[a,b,c]*, Matias Kagias[a], Joan Vila-Comamala[a,b], Konstantins Jefimovs[a,b], Li-Ting Tseng[a], Vitaliy Guzenko[a], Marco Stampanoni[a,b]

[a] *Paul Scherrer Institut, 5232 Villigen PSI, Switzerland*
[b] *Institute for Biomedical Engineering, University and ETH Zürich, 8092 Zürich, Switzerland*
[c] *Department of Physics and CNR-IMM- University of Catania, 64 via S. Sofia, Catania, Italy*
* Corresponding author

Pt de-wetting pattern

X-ray photoelectron spectroscopy (XPS) was performed to support the Pt film structure reported in Figure 2.a with the Pt-silicide formation during the annealing even at the lowest temperature (400 °C) used for applications reported in Figure 4. The sample consists of a Pt film (thickness 12 nm) deposited on air-exposed Si substrate where the native silicon oxide has not been removed before the Pt deposition, and annealed at temperature of 400 °C for 30 min in air, similar to the one reported in Figure 4.

XPS spectra are showed in Figure S1. The experimental spectrum (Figure S1.a) of Pt 4f signal can be described by metallic Pt (4f 7/2 with binding energy of 71 eV) and other species with higher binding energy relative to pure Pt. The shift to higher binding energy in PtSi and Pt_2Si are 1.7 and 1.2 eV, respectively. Both signals can contribute to the spectrum convolution. Several authors reported the following kinetics of Pt-silicide formation during annealing: the Pt_2Si phase forms at lower temperatures (180–200 °C) and is followed by the formation of the PtSi (280 - 400 °C) phase at higher temperatures. Larrieu et al. [1] showed that Pt_2Si is completely transformed in PtSi at 338 °C. However, the presence of metallic Pt in the XPS spectrum of Figure S1.a indicates that the Pt film is not completely transformed, this can be due to the presence of silicon native oxide at the interface between Si and Pt or to a low thermal budget of the process. Franco et al. [2] reported that Pt is completely transformed into PtSi at low Pt coverages (under 10 nm), annealing temperatures as high as 600 °C, and annealing times of approximately 30 min. Since the presence of metallic Pt on the surface is required to use the Pt as catalyst for MacEtch, we restricted the thermal treatment at temperature lower than 600 °C, in order to maintain a residual Pt film on the top of the catalyst layer.

The O1s signal (Figure S1.b) indicates the presence of SiO_2 (binding energy 533 eV) since Pt has been deposited on air-exposed silicon surface and the native silicon oxide has not been removed before the Pt deposition. The presence of silicon native oxide promotes the Pt film dewetting during the annealing. The nature of room temperature air grown oxide on Si substrate is different from that of the thermally grown oxide, it has been reported [3] that the initial room temperature oxide on Si cannot be represented as SiO_2 but rather as a primarily adsorbed layer of O_2. The deposition of a metal on this layer could easily break the adsorption bond and allow intimate contact with the Si substrate and the formation of Pt-silicide. While 3 nm thick thermally grown SiO2 layer works as a barrier for the formation of Pt-silicide [3].

The signal at lower binding energy relative to SiO_2 can be related to the presence of Si-(OH)x (531 eV) compounds that are formed since the sample was in humid atmosphere and the XPS analysis was not conducted in the same vacuum environment of the Pt deposition. The third peak (529.7 eV) can be related to chemisorbed oxygen on Pt surface [4] that has been incorporated during the deposition [3]. The formation of PtO_2 is excluded since it requires strongly oxidation conditions [4] and its characteristic peak at 78 eV [5] is not observed in Figure S3.a.

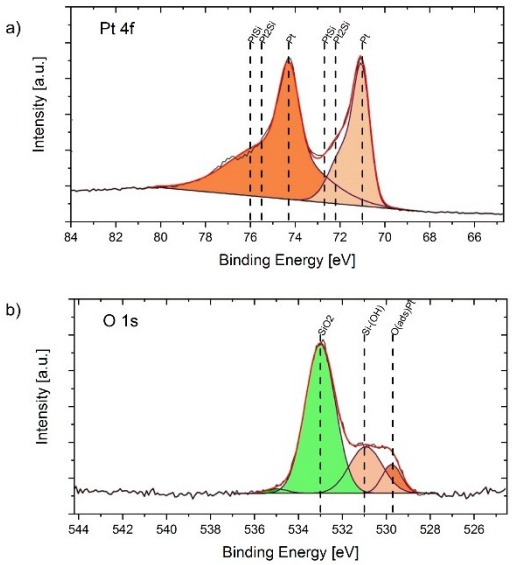

Figure S1. XPS spectra of Pt film (thickness 12 nm) on Si substrate with native silicon oxide, annealed at 400 °C in air for 30 min. a) Pt 4f, binding energy of Pt4f 7/2 and 5/2 corresponding to metal Pt, PtSi and Pt_2Si are indicated; b) O 1s, binding energy corresponding to SiO_2, Si-OH and adsorbed oxygen on Pt are indicated.

The backscattering electron (BS) image and the Energy Dispersive X-Ray Spectroscopy (EDS) were performed at 5 kV accelerating voltage to support the interpretation of conventional in-lens secondary electron (SE) image in Figure 2b (wherever not commented, the term "SEM-image" assumes the SEM image taken with in-lens SE detector). The sample consists of a Si substrate with native oxide that was deposited with Pt film (thickness 12 nm) and annealed at temperature of 550 °C for 30 min in air, similar to the one reported in Figure 2.b.

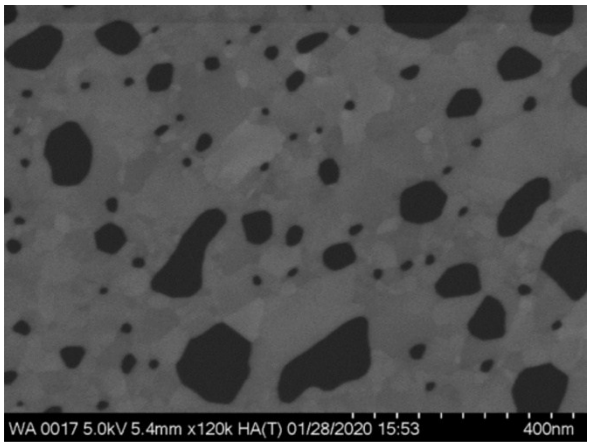

Figure S2. Backscattering electron (BS) image of Pt film (thickness 12 nm) on Si substrate after annealing at temperature of 550 °C for 30 min in air

In the BS image (Figure S2), the topographical contrast is minimized and it is possible to observe the compositional contrast of the film. The contrast grows as a function of the atomic number, therefore the brighter contrast in the BS image should correspond to Pt, as confirmed by the EDS analysis.

The EDS map is showed in Figure S3. The images was acquired in a close region of BS image to minimize the carbon contamination. EDS was conducted in a Hitachi Regulus 8230 at 5 kV accelerating voltage in order to minimize the interaction volume in the material, which determines the resolution of the EDS image, and to be able to retrieve the signal from Si and Pt. The high

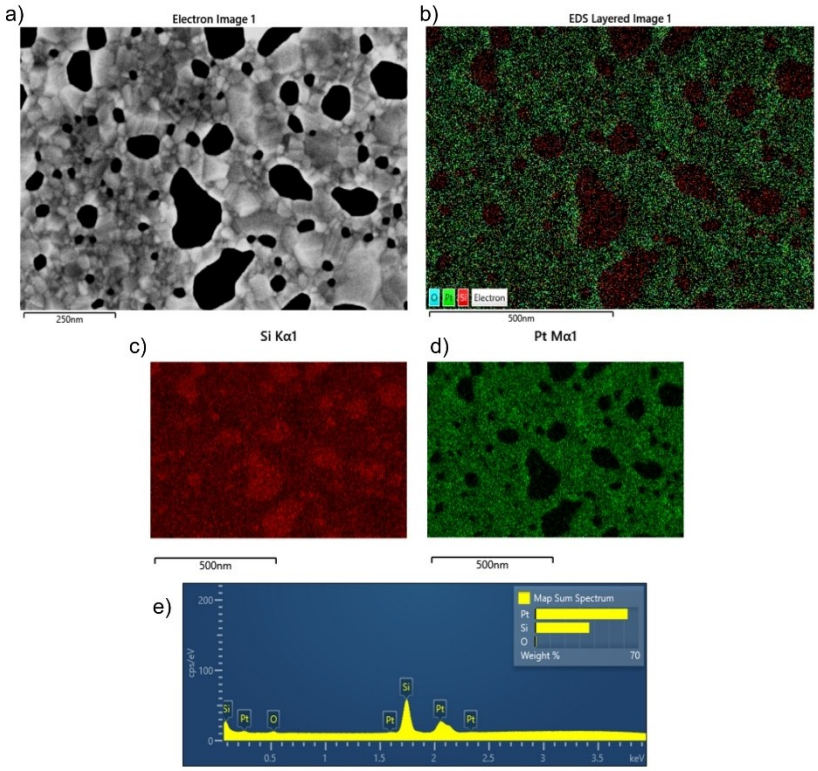

Figure S3. Energy Dispersive X-Ray Spectroscopy (EDS) of Pt film (thickness 12 nm) on Si substrate after annealing at temperature of 550 °C for 30 min in air. a) secondary electron (SE) image; b) EDS map with merged signals of Pt, Si and O; c) EDS map of Si signal (Kα 1.739 keV); d) EDS map of Pt signal (Mα1 2.048 keV); e) EDS spectrum of the mapped area.

magnification SE image (Figure S3 a) shows the topographical contrast due to the fracturing and reassembling of the Pt film as a consequence of de-wetting. The EDS spectrum is reported showing the X-ray characteristic peaks for Si (Kα 1.739 keV), Pt (Mα1 2.048 keV) and O (Kα 0.525 keV). Oxygen is present everywhere with a very weak signal so the map is not reported. The Pt film (bright contrast in SEM and BS, green in EDS map) formed a network on the Si substrate, opening holes and exposing the Si substrate (dark contrast in SEM and BS, red in EDS map) as a consequence of the thermal de-wetting process. The comparison of EDS, BS and SE images shows that Pt is localized in the brighter contrast region of SE image. The presence of Pt signal inside the holes (Pt EDS map in Figure S3.d) is due to the limited resolution of EDS map with respect of SE and BS images.

Pt catalyst without Pt-silicide

The formation of Pt –silicide helps to stabilize the metal pattern during MacEtch. The Pt silicide is formed during the thermal treatment that is used to induce the thin film de-wetting. The de-wetting forms a metal interconnected structure that is used as a catalyst pattern for etching nanowires by MacEtch. The metal film de-wetting can be induced also during deposition at room temperature if the film is thin enough. Figure S4a shows an example of metal de-wetting induced during depos7ition of Pt on oxygen terminated Si substrate, the film thickness is 8 nm. The metal pattern

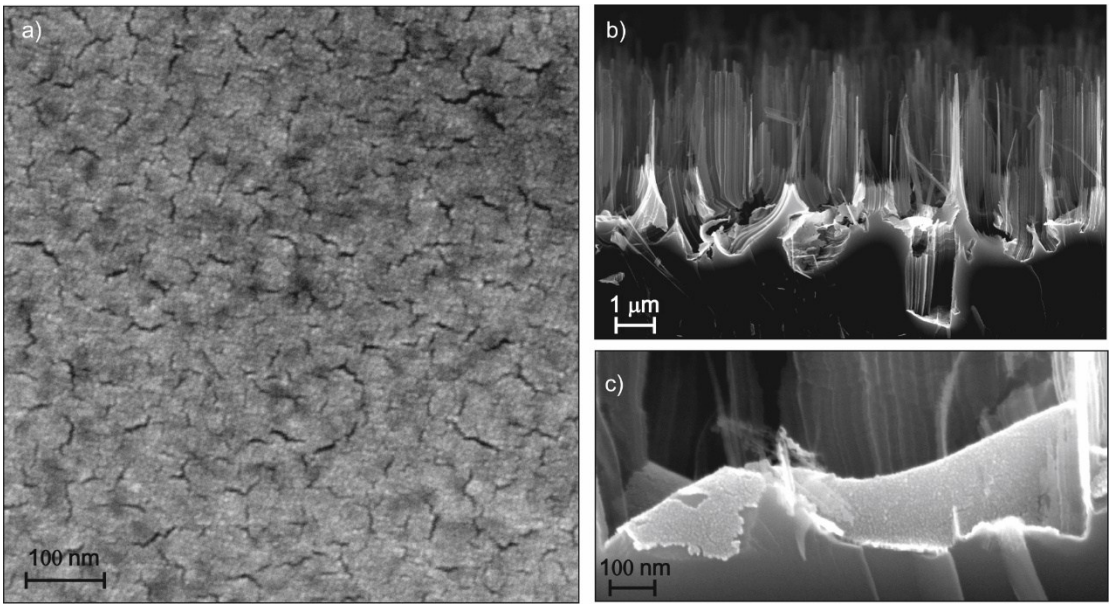

Figure S4. a) SEM plan view of Pt film (8 nm) as deposited on Si <100> substrate, the film is so thin to form clusters on Si during deposition, the black cracks are exposing Si and forms a mask for nanowires in MacEtch; b) cross section SEM image of sample in a) after 100 min of MacEtch in gas phase, nanowires are formed but the metal pattern is unstable, the pattern cracks and etch in direction out of vertical <100> in the substrate, random uncontrolled moving of the catalyst happens during etching; c) high magnification of b) showing metal film instabilities.

forms nanometric cracks that can be used as a metal mask for the formation of nanowires during MacEtch. We did not anneal the metal pattern on purpose to avoid the formation of Pt silicide. After deposition the sample was exposed to vapour HF and air at 55 °C in order to perform the MacEtch in gas phase. Vertical nanowires are formed in the first stage of MacEtch but after few micrometers of etching the metal pattern become instable and the etching proceeds in directions out of vertical <100> in the substrate. The metal patterns instabilities are visible in SEM cross section (Figure S4.b-c), the metal deteriorates and loses adhesion with the substrate.

Wet versus gas phase MacEtch for nanostructures

Figure S5 shows a comparison of nanowires formed by wet-MacEtch and MacEtch in gas phase, the images are SEM in plan view and have the same scale. The nanowires are viewed from the top and are in both cases 8 µm long with similar section size distribution. A remarkable agglomeration with the formation of large bundles is observed in wet etching (Fig. S5a) due to the liquid drying at the end of the process, while nanowires are more separated in gas phase etching (Fig. S5b). Moreover, nanowires in wet etching tends to bend when form the big bundles, while in gas phase etching the nanowires stay vertical since only the top of the pillars are visible in the SEM image (Fig. S5b).

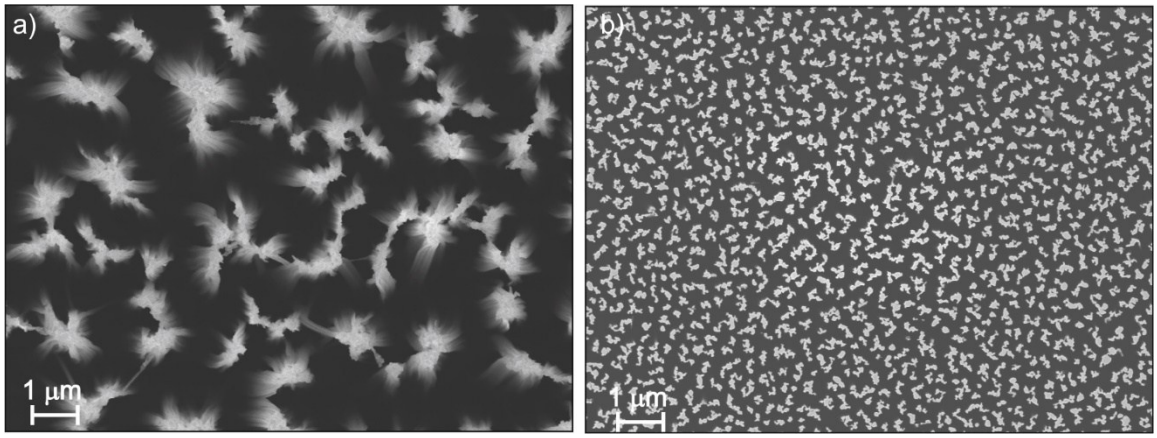

Figure S5 a) plan view SEM of nanowires etching in liquid MacEtch and then dried after the process, large bundles of nanowires are visible; b) nanowires formed by MacEtch in gas phase showing reduced agglomeration of nanowires .

H_2O_2 versus O_2 as oxidizer for MacEtch in gas phase

Figure S6 demonstrates the negligible effect of H_2O_2 as oxidizer for MacEtch in vapour phase. The liquid composition was varied by mixing HF (49 w%), H_2O_2 (30 wt%) and deionized water in different volume ratios with a total liquid volume of 100 ml. The vapor composition is determined by the partial pressure of the different liquid components. According to the Rault's law, the vapor composition is richer in the most volatile component of the liquid. We calculated the vapor composition by using the partial pressures of HF, H_2O_2, and H_2O at 300 K [6, 7]. With respect to the composition of the liquid, the molar concentration in the vapor is reduced by a factor of ~ 50 for HF and ~ 500 for H_2O_2. This means that the typical ρ parameter for the vapor is usually very high for a large range of composition of the liquid (see Figure S6a), where ρ = [HF]/([HF] +[H_2O_2]) was introduced for the first time by Chartier et al. [8]. Since the etching chamber is not hermetically closed and the system is placed on a bench under air in laminar flow, the air is continuously flowed in during the etching. We observed the same surface structuring of the sample with the same etching rate when the etching solution contains H_2O_2 or simply deionized water, indicating the negligible effect of H_2O_2 with respect of oxygen from the air. Figure S6b-c reports the SEM in cross section of the same sample etched at 55 °C in presence of H_2O_2 (50 ml H_2O_2 and 50 ml HF) or water (50 ml H_2O and 50 ml HF) in the liquid solution, respectively.

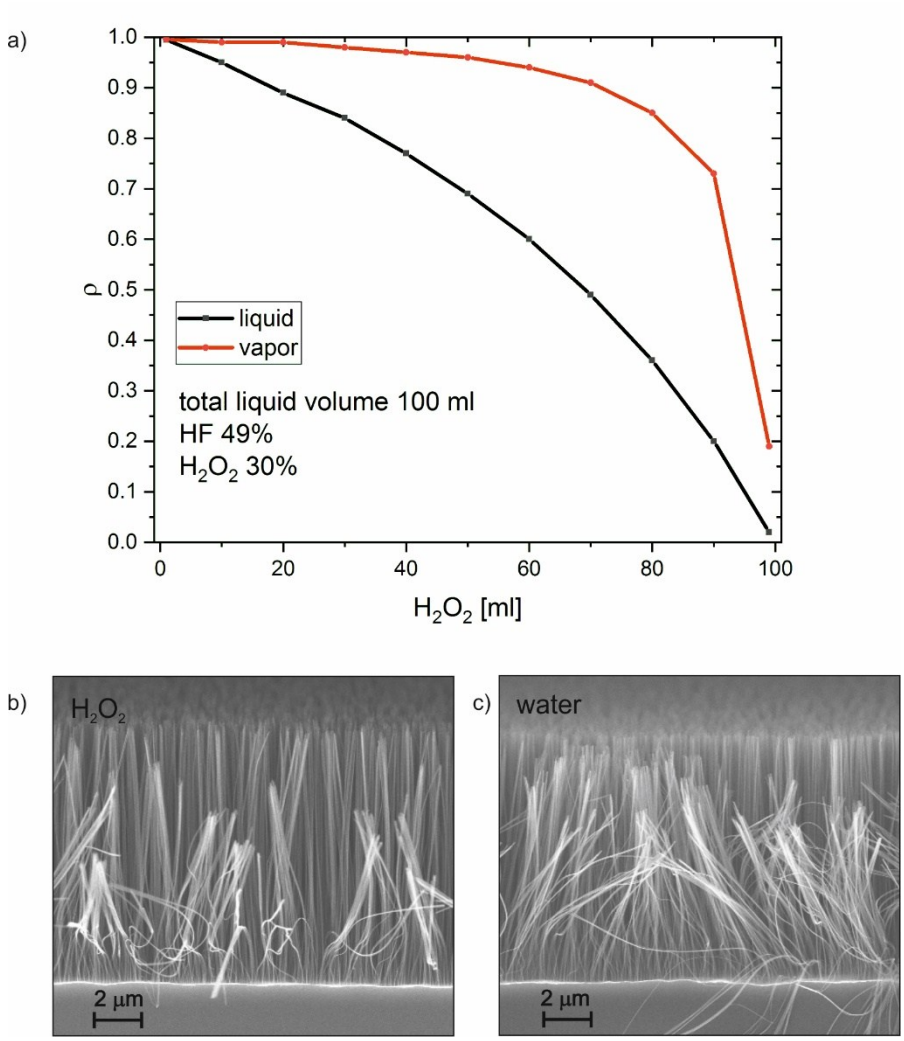

Figure S6 a) Calulated ρ (ρ = [HF]/([HF] +[H_2O_2]) for MacEtch in liquid and vapor assuming a liquid volume of 100 ml solution of water diluted HF and H_2O_2; SEM in cross section of sample exposed to vapor at 55 °C in presence of b) H_2O_2 (50 ml H_2O_2 and 50 ml HF) or c) water (50 ml H_2O and 50 ml HF) in the liquid solution.

Effect of substrate temperature on porosity

The substrate temperature during MacEtch in gas phase is a relevant parameter to control the water desorption, if the condense layer is too thick the nanostructures can be subjected to stiction. Moreover, the condensed layer also affects the structure porosity. Some tiny pores on the nanowires can be detected even by SEM at the bottom of the nanowires carpet for long etching at temperature of 40 °C (Figure S7a). The NWs porosity can be reduced by increasing the substrate temperature. The effect of the condensed layer is extremely relevant for the degradation of patterned microstructures (see Figure S7b), which appear very porous even on top when etched at temperature below 40 °C. This is because desorption is less efficient in microstructures as compared to nanowires, where the higher surface to volume aspect ratio favors a quick drying. Figure S7b shows a grating with a pitch of 2 µm etched in gas phase at temperature of 35 °C, the silicon lamellas have a thick porous layer that is not homogenous with depth and degrades the profile.

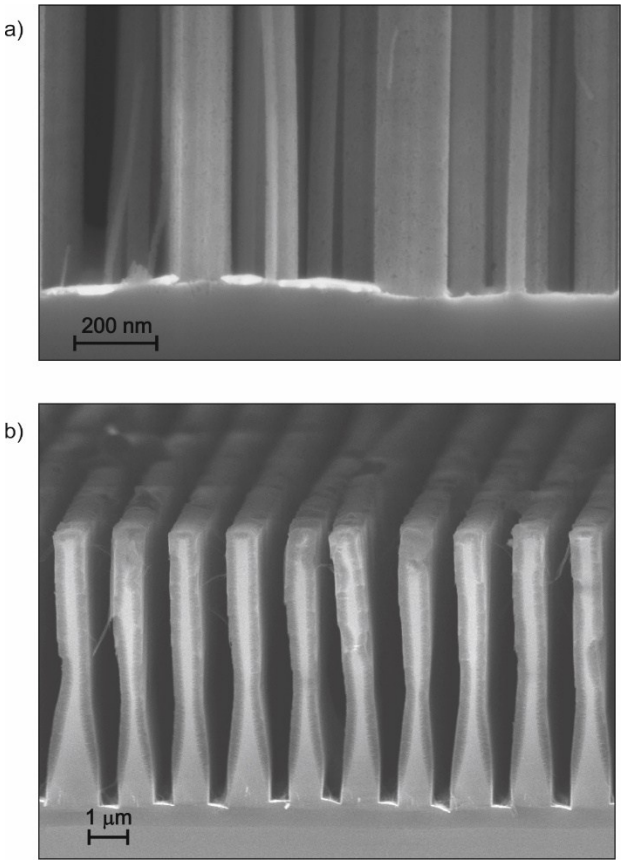

Figure S7 a) SEM cross section of bottom part of nanowires carpet etched by MacEtch in gas phase at 40 °C, tiny pores are barely visible; b) SEM cross section of grating with pitch 2 µm etched at 35 °C, the porous layer has an clear contrast with respect of bulk Si.

Porosity in gas- versus wet - MacEtch

In order to compare the Si porosity obtained by gas-MacEtch with that of regular MacEtch in liquid (wet-MacEtch), we etched one grating structure prepared on Si substrate is <100> n-type with

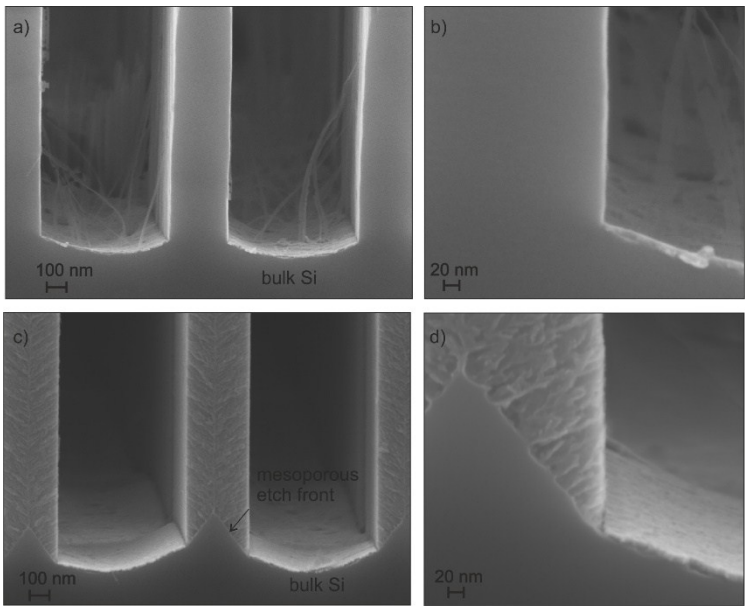

Figure S8. SEM in cross section of bottom part of grating with 1 µm pitch etched in (a-b) gas-MacEtch and in (c-d) wet-MacEtch with a liquid solution of HF and H_2O_2. The mesoporous etch front in wet-MacEtch is visible at interface with bulk Si.

resistivity 0.001-0.01 Ωcm in a liquid solution of HF (5 mol/l) and H_2O_2 (0.5 mol/l) at room temperature. The top part of the etched structures is usually more porous since it is subjected to longer exposure to etchants, therefore we used the bottom part to compare the porosity. Figure S8 reports SEM images in cross-section with high magnification of the bottom part of gratings structures with pitch 1 µm similar to those of Figure 4.e-h. Figure S8 show the structures etched in gas-MacEtch (Fig. S8 a-b) and in a liquid solution of HF and H_2O_2 (Fig. S8 c-d). SEM images have been acquired in the same session, with the working distance (3 mm) and acceleration voltage (5 kV) in order to guarantee as much as possible the same contrast conditions. The characteristic V shape of the Si lamella in Figure S8 c-d shows the mesoporous etch front and it is useful to depict the contrast variation within the same SEM image due to the porosity presence. The mesoporous etch front is not visible in the structure etched by gas-MacEtch in agreement with the Hildreth et al. observation [9], indicating that gas-MacEtch in heavily doped Si effectively produces less porous structures with respect of wet-MacEtch in liquid solution of HF and H_2O_2. The porous morphology of Si using MacEtch has been attributed to the diffusion of holes outside of the metal–semiconductor interface and causing an additional but reduced extent of etching in the areas outside the metal mesh pattern. Balasundaram et al. [10] showed that porosity depends on Si doping, the dopant atoms are thermodynamically favorable sites for the formation of pores, heavily doped Si in liquid MacEtch produces very porous structures even in conditions of very low H_2O_2 concentration. B. Zhu et al. [11] showed the morphology of the mesoporous Si layer is highly visible in SEM even when it is formed in Pt catalyzed MacEtch in liquid solution with HF 21.2 mol/l and H_2O_2 concentration of 0.18 mol/l.

Aspect ratio up to 10000:1

In the top view of the NWs carpet the visualization of the smaller nanowires is complicated because of vibration, strong signal coming from the top of the carpet and charging in high resolution. Figure

3h has been acquired with the best resolution for the top part of the NWs carpet. In order to perform higher resolution images of the NWs along the full length, we scratched the surface of the etched Si substrate showed in Figure 3e. The NWs are very flexible and not easy to break in the size range. We dispersed part of the NWs carpet on a flat aluminum substrate. The nanowires form immediately bundles since they are very sensitive to air humidity, so it almost impossible to isolate single NWs. We were able to detect few fibers lying flat on the new substrate. Once a fiber has been isolated on a separate substrate, we were able to focus on the smaller structures. The use of aluminum substrate and the adhesion of the nanowires on the new substrate were useful to minimize the charging in high resolution. Figure S9a shows SEM in plan view of a fiber composed of few (10-20) NWs. The length of the fiber is between 102 and 134 µm, the original length of the NWs carpet is measured in Figure 3e (107 um) so the fiber is lying almost flat. The measured length of 134 µm is clearly due to the unraveling of the fiber once dispersed, similar to thrown Mikado sticks. It is possible to identify the bottom and top part of the fiber (both indicated in Figure S9a) since in high magnification (Figure S9k) the porosity is similar to the one showed in top part of the NWs carpet (Figure 3h). The Figures S9b-l are collected along the length of the fiber as demonstrated by the X and Y positions of the SEM stage. SEM was used with acceleration voltage of 5 kV and smallest aperture of 10 µm so to maximize the resolution. The SEM images have high noise to signal ratio to avoid charging effects. The resolution is high enough to measure the NWs size, every image (Figures S9b-l) show the presence of features size in the range of 10 nm that can be related to real NWs with 10 nm diameter or part of more complex shapes. Unfortunately, it is not possible to follow a single NW along the full length or discriminate among the different NWs in the SEM images. However, the detected feature size is 10 nm or even less along the full length of the fiber that is extracted from a NWs carpet with thickness of 107 µm. This demonstrates that aspect ratio as high as 10000:1 can be achieved by MacEtch in gas phase.

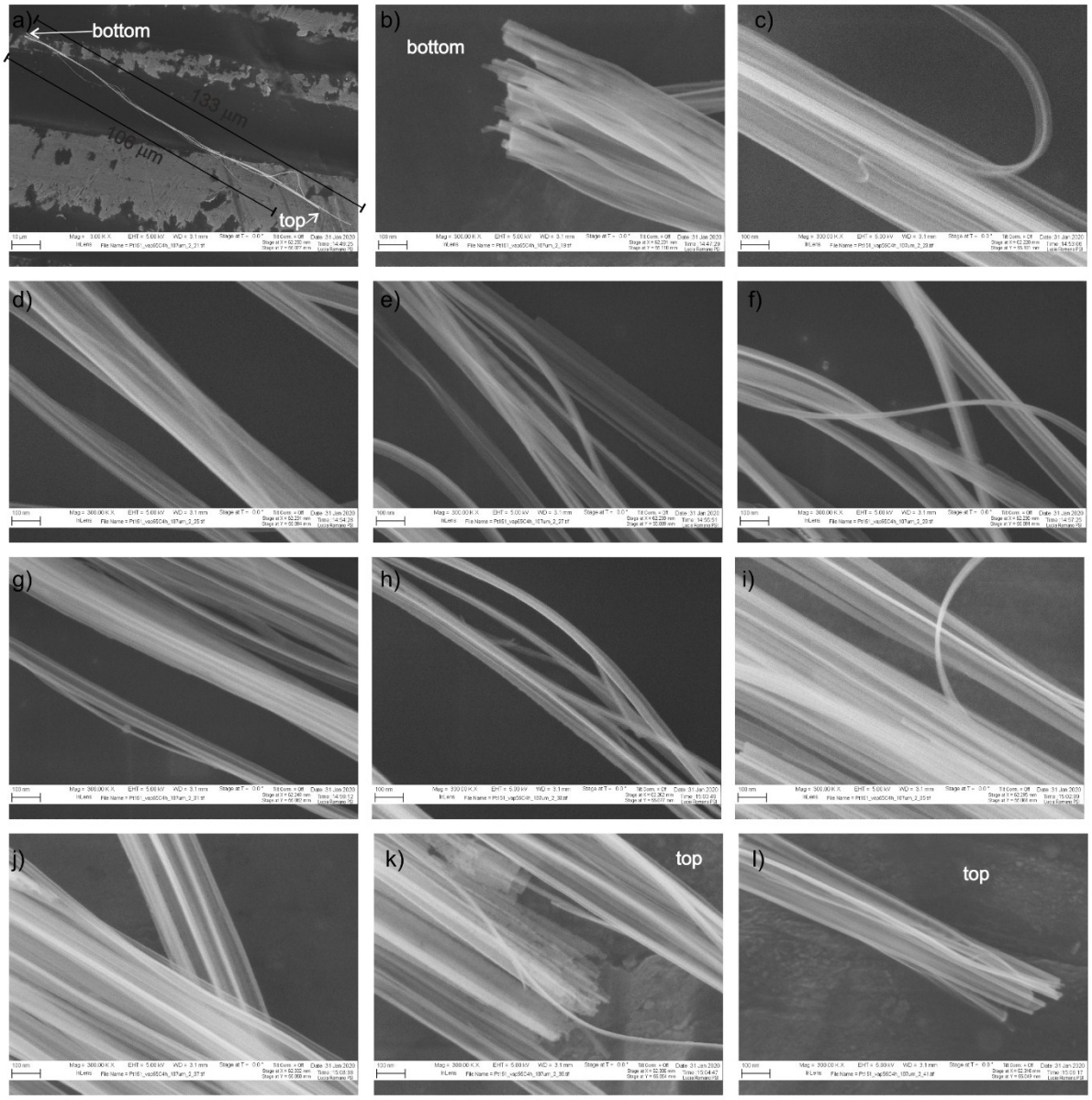

Figure S9. SEM in plan view of a fiber composed of few (10-20) NWs laying on a flat aluminium substrate. a) low magnification of the full fiber; b-l) high magnification along the whole length of the fiber, NWs with diameter of at least 10 nm are visible in all the sections of the fiber length.

Metal interconnected pattern

Figure S10 reports some examples of metal pattern before the etching. The pattern was realized by electron beam lithography, Pt thin film deposition and lift-off. The pattern was optimized to ensure the catalyst interconnection (bridges of periodic pattern) and to minimize the catalyst off-vertical movement. Figure S10a shows the metal pattern of a circular grating with pitch of 1 µm. Figure S10b shows the metal pattern of a linear grating with pitch of 200 nm, the match of pattern feature size before and after the etching indicates the quality of pattern transfer during MacEtch.

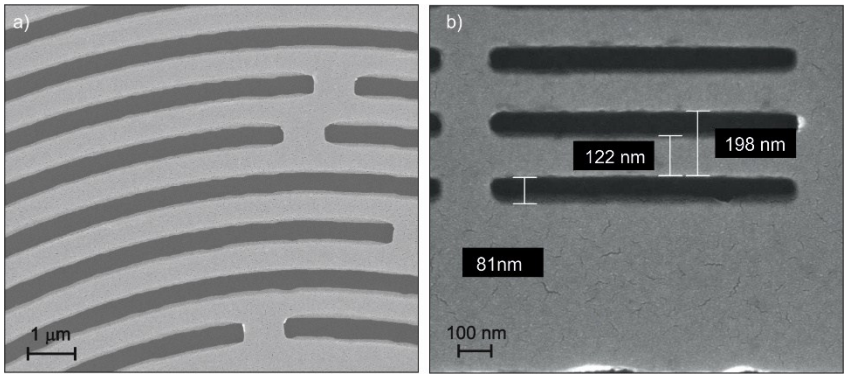

Figure S10. SEM of metal pattern realized by electron beam lithography, Pt deposition and lift-off before etching of: a) circular grating with pitch of 1 µm; b) linear grating with pitch of 200 nm with measure of the feature size before MacEtch (to be compared with Figure 4d).

X-ray Optics feature size

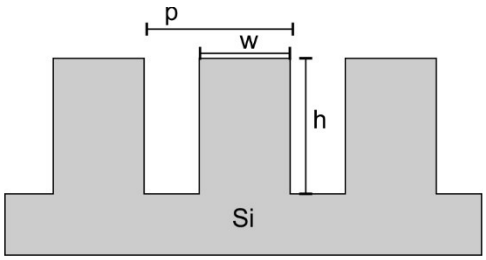

Figure S11. Schematic of etched structure in Si substrate. Aspect ratio is calculated from the ratio of etched depth h and width w of the Si lamella.

Table S1. Features sizes of the different structures reported in Figure 4. Aspect ratio is calculated from the ratio of etched depth h and width w of the Si lamella (see Figure S11).

Structure	**Figure 4**	**SEM**	**Pitch p [µm]**	**Si width w [µm]**	**Etched depth h [µm]**	**Aspect ratio**
Linear grating	b	Tilted view	20	5	6	1:1
Linear grating	c	Cross section	4.8	2.4	39	16:1
Linear grating	d	Plan view	0.2	0.08	10	125:1
Circular grating with duty cycle 0.65	e, f, g h	Tilted view Cross section Plan view	1	0.35	29	82:1
Zone plate	I, j, k	Tilted view	0.2-2	0.1-1	5	50:1 – 5:1

In plan view the Si substrate is perpendicular to the electron beam of SEM;
In cross section the Si substrate is parallel to the electron beam of SEM;
In tilted view the Si substrate is tilted of 30° with respect to the electron beam of SEM.

References in Supplementary Information

1. G. Larrieu, E. Dubois, X. Wallart, X. Baie and J. Katcki, *Journal of Applied Physics*, 2003, **94**, 7801-7810.
2. N. Franco, J. E. Klepeis, C. Bostedt, T. Van Buuren, C. Heske, O. Pankratov, T. A. Callcott, D. L. Ederer and L. J. Terminello, *Physical Review B*, 2003, **68**, 045116.
3. S. M. Goodnick, M. Fathipour, D. L. Ellsworth and C. W. Wilmsen, *Journal of Vacuum Science and Technology*, 1981, **18**, 949-954.
4. M. A. van Spronsen, J. W. M. Frenken and I. M. N. Groot, *Nature Communications*, 2017, **8**, 429.
5. Z. Li, P. Beck, D. A. A. Ohlberg, D. R. Stewart and R. S. Williams, *Surface Science*, 2003, **529**, 410-418.
6. S. L. Manatt and M. R. R. Manatt, *Chemistry – A European Journal*, 2004, **10**, 6540-6557.
7. C. R. Helms and B. E. Deal, *Journal of Vacuum Science & Technology A*, 1992, **10**, 806-811.
8. C. Chartier, S. Bastide and C. Lévy-Clément, *Electrochimica Acta*, 2008, **53**, 5509-5516.
9. O. J. Hildreth and D. R. Schmidt, *Advanced Functional Materials*, 2014, **24**, 3827-3833.
10. K. Balasundaram, S. S. Jyothi, S. Jae Cheol, A. Bruno, C. Debashis, M. Mohammad, H. Keng, A. R. John, F. Placid, S. Sanjiv and L. Xiuling, *Nanotechnology*, 2012, **23**, 305304.
11. B. Zhu, W.-J. Liu, S.-J. Ding, D. W. Zhang and Z. Fan, *The Journal of Physical Chemistry C*, 2018, **122**, 21537-21542.